

Electrochemical and Spectroscopic Effects of Mixed Substituents in Bis(phenolate)–Copper(II) Galactose Oxidase Model Complexes

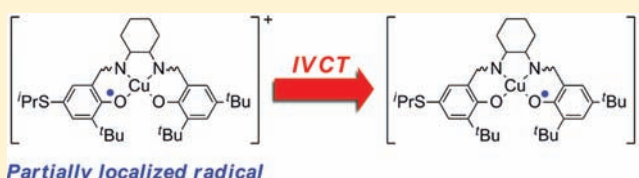
Russell C. Pratt,[†] Christopher T. Lyons,[†] Erik C. Wasinger,[‡] and T. Daniel P. Stack^{†,*}

[†]Department of Chemistry, Stanford University, Stanford, California 94305, United States

[‡]Department of Chemistry, California State University, Chico, Chico, California 95929, United States

S Supporting Information

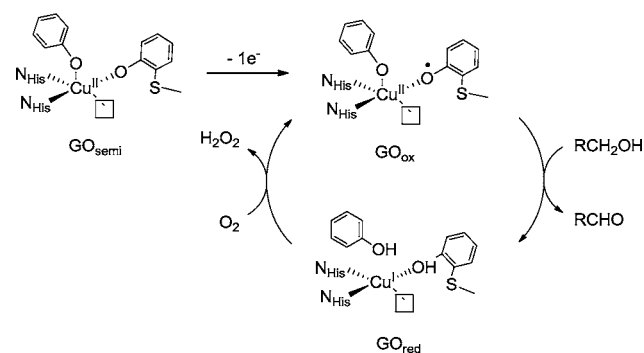
ABSTRACT: Nonsymmetric substitution of salen ($1^{R_1,R_2}$) and reduced salen ($2^{R_1,R_2}$) Cu^{II}–phenoxyl complexes with a combination of ^tBu, ⁱPr, and ^oMe substituents leads to dramatic differences in their redox and spectroscopic properties, providing insight into the influence of the cysteine-modified tyrosine cofactor in the enzyme galactose oxidase (GO). Using a modified Marcus–Hush analysis, the oxidized copper complexes are characterized as Class II mixed-valent due to the electronic differentiation between the two substituted phenolates. Sulfur K-edge X-ray absorption spectroscopy (XAS) assesses the degree of radical delocalization onto the single sulfur atom of nonsymmetric [$1^{Bu,SMe}$]⁺ at 7%, consistent with other spectroscopic and electrochemical results that suggest preferential oxidation of the ^oMe bearing phenolate. Estimates of the thermodynamic free-energy difference between the two localized states (ΔG°) and reorganizational energies (λ_{R_1,R_2}) of [$1^{R_1,R_2}$]⁺ and [$2^{R_1,R_2}$]⁺ lead to accurate predictions of the spectroscopically observed IVCT transition energies. Application of the modified Marcus–Hush analysis to GO using parameters determined for [$2^{R_1,R_2}$]⁺ predicts a ν_{max} of $\sim 13600\text{ cm}^{-1}$, well within the energy range of the broad Vis–NIR band displayed by the enzyme.



INTRODUCTION

The enzyme galactose oxidase (GO) catalyzes the two-electron, two-proton oxidation of primary alcohols to aldehydes with concomitant two-electron, two-proton reduction of dioxygen to hydrogen peroxide.^{1,2} The active site contains a mononuclear copper center ligated by two equatorial histidines, one axial unmodified tyrosine, and an equatorial tyrosine that is covalently cross-linked to a neighboring cysteine residue in an oxidative post-translational modification (Scheme 1).^{3–5}

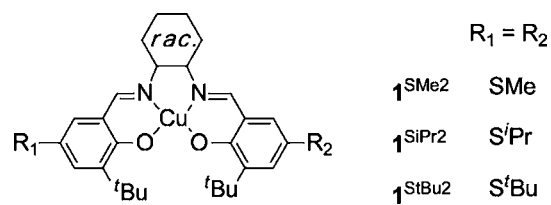
Scheme 1. Active Site and Consensus Mechanism of GO



The two catalytically relevant forms, reduced (GO_{red}) and oxidized (GO_{ox}), contain a Cu^I–tyrosine unit and a Cu^{II}–cysteine modified tyrosyl radical, respectively, while the inactive semireduced form (GO_{semi}) exists as a Cu^{II}–tyrosine species.

Delocalization of the tyrosyl radical onto the thioether bridge, which is predicted by density functional theory (DFT) computations^{6,7} and EPR studies of copper-free GO,⁸ is postulated to contribute to the energetic stabilization of GO_{ox} ($t_{1/2} = 7.2$ days).¹ We have recently reported a detailed analysis of the electrochemical and spectroscopic properties of a series of symmetric *para*-alkylsulfanyl substituted Cu^{II}–bis-imine, bis-phenolate model complexes (1^{SR_2} , Scheme 2) and have

Scheme 2. Structure of 1^{SR_2}

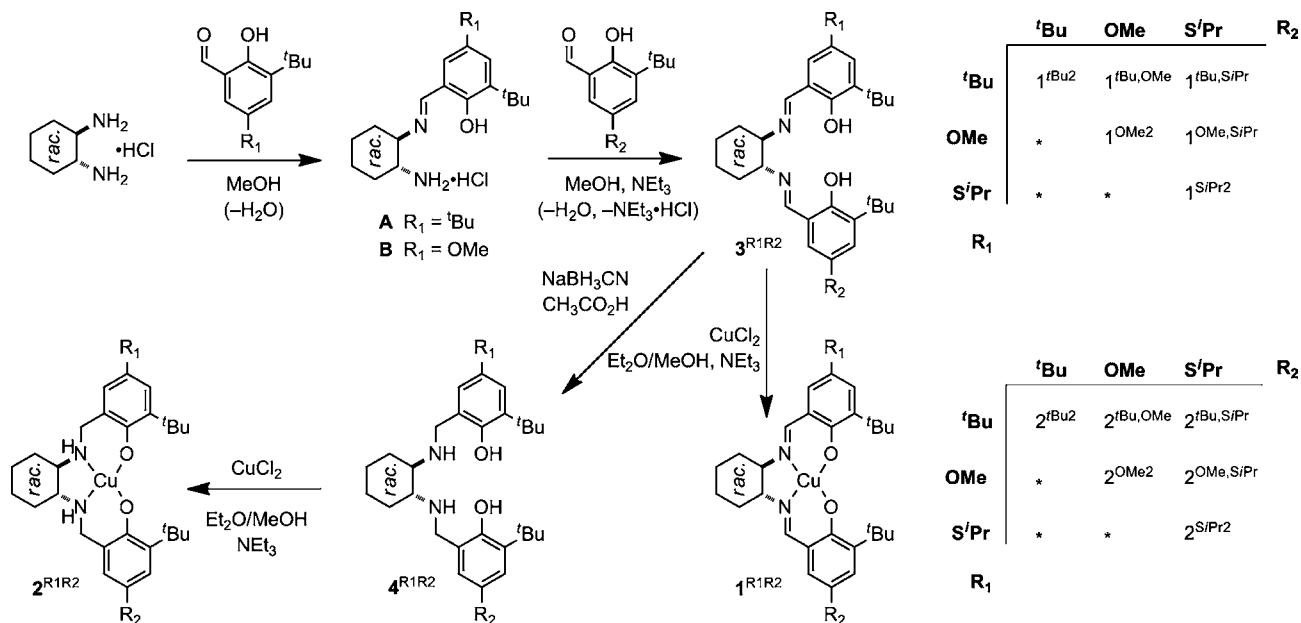


quantified the degree of radical delocalization onto the sulfur atoms using sulfur K-edge X-ray absorption spectroscopy (XAS).⁹

Several examples of GO model complexes of tripodal ligands containing two different phenolates exist in the literature.^{10–12} Access to nonsymmetric salen-like ligands was problematic until a two-step procedure was reported by Campbell and Nguyen.¹³ Such ligands allow for exploration of the impact of the electronic asymmetry of nonsymmetric salen metal complexes in catalysts

Received: December 1, 2011

Published: April 3, 2012

Scheme 3. Synthetic Scheme for Cu^{II}–Phenolate Complexes

and materials,^{14–17} and provide access to model complexes possessing greater structural and electronic fidelity to GO.

Wen and co-workers have used titanium–salen complexes, nonsymmetrically substituted with Lewis basic substituents for the cyanosilation of aldehydes.¹⁸ Herrero and co-workers have reported the decoration of a Mn(III)–salen complex with a Ru photosensitizer, which results in light induced oxidation to a Mn(IV) high-spin intermediate.¹⁹ Nakano and co-workers have shown the use of nonsymmetric Cr–salen complexes containing either reduced or substituted imine bonds as epoxide-CO₂ copolymerization catalysts.²⁰ Kochem and co-workers have investigated the effect of substituent protonation on the locus of oxidation in nonsymmetric Ni–salen complexes.²¹ Recently, Kurahashi and Fujii reported the study of one-electron oxidized nonsymmetric Mn– and Ni–salen complexes using a similar approach to the one presented here.²²

The thioether modification within GO model complexes generally focuses on *ortho*-alkylsulfanyl substituted phenolates. In this work, complexes purposefully bearing a single alkylsulfanyl substituent in the *para* position are examined (Scheme 3); the *para* positioning assures minimal copper coordination changes within the series of complexes with sterically abutting *ortho*-*t*-butyl substituents on the phenolates. To generalize the results, the scope of this study was expanded in two ways: first, in addition to *tert*-butyl (^tBu) and isopropylsulfanyl (ⁱPr) substituents, phenolates with methoxy (^{OMe}) substituents are included in this study.^{23,24} Second, the 2^{R₁R₂} analogs of 1^{R₁R₂} wherein the two carbon–nitrogen imine bonds in the ligand backbone are reduced have been characterized in parallel. The 2^{R₁R₂} complexes display electrochemical and spectroscopic features similar to those observed for 1^{R₁R₂}, and reduction of the imines helps to clarify the near-UV optical transitions by eliminating transitions within the imine functional groups.²⁵ The set of testable systems is therefore greatly expanded. Complexes with identical phenolates will be referred to as “symmetric” complexes, while complexes with combinations of ^tBu, ⁱPr, and ^{OMe} substituents will be referred to as “nonsymmetric” complexes.

GO_{ox} and [1^{SR₂}]⁺ (Scheme 2) are mixed-valent species in which the π -orbitals of the phenolate and phenoxyl radical rings

comprise redox-active centers that are bridged by *d*-orbitals of the Cu^{II} center. In [1^{SR₂}]⁺, the π -orbitals of the parent phenolate rings are iso-energetic and the radical hole could fully localize on one ring (Class I), partially localize (Class II), or fully delocalize over both rings (Class III), following the Robin-Day classification scheme.^{26–28} We have shown previously that subtle ligand perturbations can lead to radical localization on electron rich phenolate moieties in salen-metal complexes.²⁹ Extending this idea to phenolates bearing *para* substituents, we expect the radical to localize on the phenolate bearing the most electron-donating substituent (i.e., ^{OMe} > ⁱPr > ^tBu). A Marcus–Hush analysis of the NIR absorptions of [1^{SR₂}]⁺, attributed to intervalence charge transfer (IVCT) transitions, suggests that these complexes are best described as Class II mixed-valent.⁹ This transition between two ligands in distinct oxidation states may also be described as ligand-to-ligand charge transfer.³⁰ A similar conclusion results for the nonsymmetric complexes with a free-energy driving force for partial radical localization on the phenolate bearing the more electron-donating substituent.⁹ Sulfur K-edge X-ray absorption spectroscopy (XAS) probes the amount of hole delocalization onto the sulfur atom of a complex most structurally relevant to GO_{ox}, verifying the locus of oxidation on the sulfanyl substituted phenolate moiety.

EXPERIMENTAL DETAILS

Materials and Methods. Reagents and solvents were commercially available and used as received unless noted otherwise. Triethylamine was distilled from CaH₂ and methanol was dried using activated 3 Å molecular sieves prior to use. 3-*tert*-butyl-5-methoxysalicylaldehyde,³¹ 3-*tert*-butyl-5-isopropylsulfanylsalicylaldehyde, 3-*tert*-butyl-5-methylsulfanylsalicylaldehyde, 3^{SⁱPr}, and 1^{SⁱPr} were synthesized by reported procedures.²⁵ ¹H NMR spectra were obtained on a Varian XL-400 spectrometer operating at 400 MHz; all samples were dissolved in CDCl₃. Cyclic voltammetry was performed using a BAS CV-40 potentiometer, a AgCl/Ag wire reference electrode, a graphite disk working electrode, and a Pt wire counter electrode with 0.1 M Bu₄NClO₄ solutions in CH₂Cl₂; ferrocene or decamethylferrocene (*E*_{1/2}^o = –530 mV vs Fc⁺/Fc) was added as an internal standard. Electronic (UV–vis–NIR) spectra were collected using a Cary 50 split

beam spectrophotometer (190–1100 nm) or a Cary 500 dual beam spectrophotometer (300–3300 nm). X-band EPR spectra were obtained using a Bruker EMX spectrometer, a ER041XG microwave bridge and ER4102ST cavity, with samples held in a liquid nitrogen-filled finger dewar; EPR intensities refer to values obtained by double-integration of the first harmonic spectrum. Mass spectral services were provided by the Mass Spectrometry Facility of the University of California, San Francisco (MALDI-TOF and ESI) or by Stanford University Mass Spectrometry (ESI).

3^{OMe2}. To a solution of 3-*tert*-butyl-5-methoxysalicylaldehyde (416 mg, 2.0 mmol) in 7.5 mL methanol was added racemic *trans*-1,2-diaminocyclohexane (120 μ L, 114 mg, 1.0 mmol). The solution was heated to reflux for 10 min, then cooled and left to stand at -20 °C for 2 h. The resulting precipitate was isolated by filtration and washed with cold methanol. Yield: 440 mg (91%) of a yellow solid. ¹H NMR: δ 13.50 (s, 2H, OH), 8.24 (s, 2H, CH=N), 6.89 (d, J = 3.0 Hz, 2H, ArH), 6.47 (d, J = 3.0 Hz, 2H, ArH), 3.68 (s, 6H, OCH₃), 3.31 (m, 2H, N-CyH), 2.0–1.2 (br m, 6H, CyH), 1.39 (s, 18H, C(CH₃)₃). ESI-MS: m/z 495 (M + 1).

N-(3,5-di-*tert*-butyl-2-hydroxybenzylidene)-*trans*-1,2-diaminocyclohexane hydrochloride (A). The following procedure is adapted from that of Campbell and Nguyen.¹³ To a solution of NH₄Cl (161 mg, 3.0 mmol) in dry methanol (10 mL) was added racemic *trans*-1,2-diaminocyclohexane (360 μ L, 342 mg, 3.0 mmol). The solvent was removed under reduced pressure to give racemic *trans*-1,2-diaminocyclohexane monohydrochloride in quantitative yield (452 mg, corresponding to loss of 1 eq of NH₃). The hydrochloride salt was then redissolved in dry methanol (10 mL) and a solution of 3,5-di-*tert*-butylsalicylaldehyde (702 mg, 3.0 mmol) in dry methanol (15 mL) was added. After stirring for 5 min, the solvent was removed under reduced pressure to give a yellow syrup. Ether (5 mL) was added to induce precipitation of a white solid. After addition of another 20 mL of ether, the solid was isolated by filtration, washed with ether, washed with water, and then washed again with ether to give A as a white solid. Yield: 820 mg (75%).

N-(3-*tert*-butyl-2-hydroxy-5-methoxybenzylidene)-*trans*-1,2-diaminocyclohexane hydrochloride (B). This compound was synthesized by the same procedure used for A, using instead 3-*tert*-butyl-5-methoxysalicylaldehyde (208 mg, 1 mmol scale). Yield: 200 mg (59%) of a light-orange solid.

3^{Bu,OMe}. To a solution of A (183 mg, 0.50 mmol) in dry methanol (5 mL) was added a solution of 3-*tert*-butyl-5-methoxysalicylaldehyde (104 mg, 0.50 mmol) and triethylamine (140 μ L, 101 mg, 1.0 mmol) in 5 mL methanol at room temperature (RT). The solvent was then removed under reduced pressure. The resulting yellow solid was purified by column chromatography (5% ethyl acetate/hexanes on silica) to obtain the desired product. Yield: 130 mg (50%) of a yellow solid. ¹H NMR: δ 13.71 (s, 1H, ArOH), 13.48 (s, 1H, ArOH), 8.27 (s, 1H, ArCH=N), 8.24 (s, 1H, ArCH=N), 7.30 (d, J = 2.3 Hz, 1H, ArH), 6.95 (d, J = 2.4 Hz, 1H, ArH), 6.88 (d, J = 3.0 Hz, 1H, ArH), 6.46 (d, J = 3.0 Hz, 1H, ArH), 3.67 (s, 3H, ArOCH₃), 3.30 (m, 2H, N-CyH), 2.0–1.2 (br m, 6H, CyH), 1.41 (s, 9H, C(CH₃)₃), 1.39 (s, 9H, C(CH₃)₃), 1.23 (s, 9H, C(CH₃)₃). MALDI-TOF-MS: m/z 521 (M + 1).

3^{Bu,SPr}. This compound was synthesized and purified by the same procedure used for 3^{Bu,OMe}, using instead 3-*tert*-butyl-5-isopropylsulfanylsalicylaldehyde (126 mg, 0.50 mmol). Yield: 140 mg (49%) of a yellow solid. ¹H NMR: δ 14.09 (s, 1H, ArOH), 13.65 (s, 1H, ArOH), 8.29 (s, 1H, ArCH=N), 8.24 (s, 1H, ArCH=N), 7.34 (d, J = 2.2 Hz, 1H, ArH), 7.31 (d, J = 2.3 Hz, 1H, ArH), 7.13 (d, J = 2.2 Hz, 1H, ArH), 6.97 (d, J = 2.4 Hz, 1H, ArH), 3.33 (m, 2H, N-CyH), 3.06 (septet, J = 6.6 Hz, 1H, SCHMe₂), 2.0–1.2 (br m, 6H, CyH), 1.41 (s, 9H, C(CH₃)₃), 1.39 (s, 9H, C(CH₃)₃), 1.23 (s, 9H, C(CH₃)₃), 1.17 (d, J = 6.6 Hz, 6H, CH(CH₃)₂). ESI-MS: m/z 565 (M + 1).

3^{OMe,SPr}. This compound was synthesized and purified by the same procedure used for 3^{Bu,OMe}, using instead B (170 mg, 0.50 mmol) and 3-*tert*-butyl-5-isopropylsulfanylsalicylaldehyde (126 mg, 0.50 mmol). Yield: 167 mg (62%) of a yellow solid. ¹H NMR: δ 14.07 (s, 1H,

ArOH), 13.41 (s, 1H, ArOH), 8.23 (s, 1H, ArCH=N), 8.22 (s, 1H, ArCH=N), 7.34 (d, J = 2.1 Hz, 1H, ArH), 7.11 (d, J = 2.2 Hz, 1H, ArH), 6.89 (d, J = 3.0 Hz, 1H, ArH), 6.46 (d, J = 3.0 Hz, 1H, ArH), 3.68 (s, 3H, ArOCH₃), 3.32 (m, 2H, N-CyH), 3.04 (septet, J = 6.6 Hz, 1H, SCHMe₂), 2.0–1.2 (br m, 6H, CyH), 1.39 (s, 18H, overlapping C(CH₃)₃), 1.16 (d, J = 6.7 Hz, 6H, CH(CH₃)₂). MALDI-TOF-MS: m/z 543 (M + 1).

4^{OMe2}. 3^{OMe2} (90 mg, 0.18 mmol) and sodium cyanoborohydride (29 mg, 0.45 mmol) were placed in a test tube and acetic acid (0.75 mL) was added. The resulting suspension was stirred for 5 min, after which 0.75 mL of methanol were added and stirring was continued for another 30 min. The solution was then diluted with 10 mL of water, neutralized with 1 M potassium hydroxide (~15 mL) and extracted with ether (2 \times 5 mL). The ether solution was washed with saturated aqueous sodium bicarbonate (5 mL), then dried over anhydrous K₂CO₃, filtered and evaporated to give an off-white solid. Yield: 90 mg (98%). ¹H NMR: δ 6.79 (d, J = 2.9 Hz, 2H, ArH), 6.43 (d, J = 2.7 Hz, 2H, ArH), 4.03 (d, J = 13.2 Hz, 2H, Ar-CH₂H_b-N), 3.90 (d, J = 13.5 Hz, 2H, Ar-CH₂H_b-N), 3.75 (s, 6H, ArOCH₃), 2.4–1.2 (br m, 8H, CyH), 1.36 (s, 18H, C(CH₃)₃). ESI-MS: m/z 499 (M + 1).

4^{SPr2}. This compound was synthesized by the same procedure used for 4^{OMe2} using 3^{SPr2} (100 mg, 0.17 mmol) as the starting material. Yield: 90 mg (88%) of a white solid. ¹H NMR: δ 7.28 (d, J = 2.0 Hz, 2H, ArH), 6.99 (d, J = 2.0 Hz, 2H, ArH), 4.04 (d, J = 13.7 Hz, 2H, Ar-CH₂H_b-N), 3.90 (d, J = 13.5 Hz, 2H, Ar-CH₂H_b-N), 3.13 (septet, J = 6.5 Hz, 2H, SCHMe₂), 2.4–1.2 (br m, 8H, CyH), 1.34 (s, 18H, C(CH₃)₃), 1.23 (d, J = 6.5, 12H, CH(CH₃)₂). MALDI-TOF-MS: m/z 648 (M + 1).

4^{Bu,OMe}. This compound was synthesized by the same procedure used for 4^{OMe2} using 3^{Bu,OMe} (65 mg, 0.13 mmol) as the starting material. Yield: 62 mg (95%) of an off-white solid. ¹H NMR: δ 7.22 (d, J = 2.4 Hz, 1H, ArH), 6.87 (d, J = 2.3 Hz, 1H, ArH), 6.79 (d, J = 3.0 Hz, 1H, ArH), 6.44 (d, J = 3.0 Hz, 1H, ArH), 4.06 (d, J = 13.4 Hz, 1H, Ar-CH₂H_b-N), 4.01 (d, 13.6 Hz, 1H, Ar-CH₂H_b-N), 3.92 (d, J = 13.5 Hz, 1H, Ar-CH₂H_b-N), 3.90 (d, J = 13.2 Hz, 1H, Ar-CH₂H_b-N), 3.75 (s, 3H, ArOCH₃), 2.4–1.2 (br m, 8H, CyH), 1.38 (s, 9H, C(CH₃)₃), 1.36 (s, 9H, C(CH₃)₃), 1.29 (s, 9H, C(CH₃)₃). ESI-MS: 525 (M + 1).

4^{Bu,SPr}. This compound was synthesized by the same procedure used for 4^{OMe2} using 3^{Bu,SPr} (70 mg, 0.13 mmol) as the starting material. Yield: 67 mg (96%) of a white solid. ¹H NMR: δ 7.28 (d, J = 2.1 Hz, 1H, ArH), 7.22 (d, J = 2.4 Hz, 1H, ArH), 6.99 (d, J = 2.0 Hz, 1H, ArH), 6.87 (d, J = 2.3 Hz, 1H, ArH), 4.07 (d, J = 13.4 Hz, 1H, Ar-CH₂H_b-N), 4.01 (d, J = 13.4 Hz, 1H, Ar-CH₂H_b-N), 3.91 (d, J = 13.6 Hz, 1H, Ar-CH₂H_b-N), 3.89 (d, J = 13.4 Hz, 1H, Ar-CH₂H_b-N), 3.13 (septet, J = 6.7 Hz, 1H, SCHMe₂), 2.4–1.2 (br m, 8H, CyH), 1.36 (s, 9H, C(CH₃)₃), 1.35 (s, 9H, C(CH₃)₃), 1.28 (s, 9H, C(CH₃)₃), 1.23 (d, J = 6.6 Hz, 6H, CH(CH₃)₂). MALDI-TOF-MS: m/z 569 (M + 1).

4^{OMe,SPr}. This compound was synthesized by the same procedure used for 4^{OMe2} using 3^{OMe,SPr} (67 mg, 0.13 mmol) as the starting material. Yield: 61 mg (91%) of a white solid. ¹H NMR: δ 7.28 (d, J = 2.2 Hz, 1H, ArH), 6.99 (d, J = 2.0 Hz, 1H, ArH), 6.79 (d, J = 3.0 Hz, 1H, ArH), 6.43 (d, J = 2.9 Hz, 1H, ArH), 4.05 (d, J = 13.5 Hz, 1H, Ar-CH₂H_b-N), 4.02 (d, J = 13.4 Hz, 1H, Ar-CH₂H_b-N), 3.90 (d, J = 13.6 Hz, 1H, Ar-CH₂H_b-N), 3.89 (d, J = 13.6 Hz, Ar-CH₂H_b-N), 3.74 (s, 3H, ArOCH₃), 3.13 (septet, J = 6.6 Hz, 1H, SCHMe₂), 2.4–1.2 (br m, 8H, CyH), 1.35 (s, 9H, C(CH₃)₃), 1.34 (s, 9H, C(CH₃)₃), 1.24 (d, J = 6.6 Hz, 6H, CH(CH₃)₂).

1^{OMe2}. To a solution of 3^{OMe2} (150 mg, 0.30 mmol) in ether (5 mL) was added a solution of Cu(CH₃CO₂)₂·H₂O (61 mg, 0.30 mmol) in methanol (5 mL) and NEt₃ (100 μ L, 70 mg, 0.70 mmol). The volume of the mixture was reduced under vacuum, and the resulting precipitate was isolated by filtration, washed with methanol and ether, and dried in vacuum. Yield: 148 mg (88%) of a brown powder. Calculated

(found) for $C_{30}H_{40}CuN_2O_4 \cdot H_2O$: C 62.75 (62.99); H 7.37 (7.35); N, 4.88 (4.63). ESI-MS: m/z 556 ($M(^{63}Cu) + 1$).

1^{Bu,OMe}. To a solution of **3^{Bu,OMe}** (50 mg, 96 μ mol) and NEt_3 (40 μ L, 30 mg, 300 μ mol) in dry ether (2 mL) was added a solution of anhydrous $CuCl_2$ (13 mg, 100 μ mol) in dry methanol (1 mL). After stirring briefly, a precipitate formed, which was removed by filtration, washed with methanol and ether, and dried in vacuum. Yield: 37 mg (66%) of a brown solid. ESI-MS: m/z 582 ($M(^{63}Cu) + 1$).

1^{Bu,SPr}. To a solution of **3^{Bu,SPr}** (50 mg, 89 μ mol) and NEt_3 (40 μ L, 30 mg, 300 μ mol) in dry ether (2 mL) was added a solution of anhydrous $CuCl_2$ (13 mg, 100 μ mol) in dry methanol (1 mL). After a brief stirring, the ether was removed under reduced pressure, and the resulting precipitate was isolated by filtration, washed with methanol, and dried in vacuum. Yield: 46 mg (83%) of fine brown needles. MALDI-TOF-MS: m/z 626 ($M(^{63}Cu) + 1$).

1^{OMe,SPr}. This compound was prepared by the same procedure used for **1^{Bu,OMe}** using instead the precursor **3^{OMe,SPr}** (50 mg, 93 μ mol). Yield: 48 mg (86%) of a green solid. ESI-MS: m/z 599 ($M(^{63}Cu)$).

2^{OMe2}. To a solution of **4^{OMe2}** (50 mg, 0.10 mmol) and NEt_3 (40 μ L, 30 mg, 0.3 mmol) in ether (1 mL) was added a solution of anhydrous $CuCl_2$ (13 mg, 0.10 mmol) in dry methanol (2 mL). The solvent was promptly removed under reduced pressure. The solid residue that resulted was washed with ethyl acetate (5 mL), and the washings were filtered and evaporated. This residue was suspended in ether (1 mL), and hexanes (5 mL) were added to aid precipitation of a green solid that was isolated by filtration, washed with hexanes, and dried *in vacuo*. Yield: 38 mg (68%). Calculated (found) for $C_{30}H_{44}CuN_2O_4$: C 64.32 (64.07); H 7.92 (7.69); N, 5.00 (4.76). ESI-MS: m/z 560 ($M(^{63}Cu) + 1$).

2^{SPr2}. The method used to synthesize **2^{OMe2}** was used to synthesize this compound, using instead **4^{SPr2}** (50 mg, 0.09 mmol) as the ligand precursor. Yield: 46 mg (84%) of a green solid. Calculated (found) for $C_{34}H_{52}CuN_2O_2S_2$: C 62.97 (63.09); H 8.08 (7.89); N 4.32 (4.55). MALDI-TOF-MS: m/z 648 ($M(^{63}Cu) + 1$).

2^{Bu,OMe}. The method used to synthesize **2^{OMe2}** was used to synthesize this compound, using instead **4^{Bu,OMe}** (50 mg, 0.09 mmol) as the ligand precursor. Yield: 37 mg (66%) of a green solid. ESI-MS: m/z 586 ($M(^{63}Cu) + 1$).

2^{Bu,SPr}. The method used to synthesize **2^{OMe2}** was used to synthesize this compound, using instead **4^{Bu,SPr}** (50 mg, 0.09 mmol) as the ligand precursor. Yield: 32 mg (58%) of a green solid. MALDI-TOF-MS: m/z 630 ($M(^{63}Cu) + 1$).

2^{OMe,SPr}. The method used to synthesize **2^{OMe2}** was used to synthesize this compound, using instead **4^{OMe,SPr}** (50 mg, 0.09 mmol) as the ligand precursor. Yield: 17 mg (31%) of a green solid. ESI-MS: m/z 604 ($M(^{63}Cu) + 1$).

Spectrophotometric Titrations. A saturated solution of thianthrenyl hexafluoroantimonate ($Th^{*+} SbF_6^-$; ca. 0.4 mM) was freshly generated by stirring ~ 20 mg $Th^{*+} SbF_6^-$ in 10 mL CH_2Cl_2 for 30 min at RT under N_2 . Concentration of Th^{*+} in solution was determined by spectrophotometric titration of cobaltocene ($\epsilon_{30300} = 7600 M^{-1} cm^{-1}$). Spectra (3050–35000 cm^{-1}) were obtained for 0.1 mM CH_2Cl_2 solutions of **1^{R1,R2}** and **2^{R1,R2}**. Aliquots (100 μ L) of the Th^{*+} solution were then added and spectra were acquired after each addition until no further spectral changes occurred or excess Th^{*+} ($\epsilon_{18200} = 8500 M^{-1} cm^{-1}$) became apparent. Spectra were corrected for dilution. Spectra with the maximal NIR absorption were taken to best represent spectra of **[1^{R1,R2}]⁺** and **[2^{R1,R2}]⁺**, and spectra with maximal visible absorptions (ca. 16000 cm^{-1}) were taken to best represent spectra of **[1^{R1,R2}]²⁺** and **[2^{R1,R2}]²⁺**.

EPR Sample Preparation. Solutions of **1^{R1,R2}** and **2^{R1,R2}** (0.1 mM in CH_2Cl_2) were titrated spectrophotometrically (at RT or 200 K) with freshly prepared saturated solutions of Th^{*+} while being monitored in the visible region to determine end point for formation of the oxidized species. Aliquots of the titrated solutions were then transferred to

quartz tubes and frozen in LN_2 . Samples of **1^{R1,R2}** and **2^{R1,R2}** were measured under the same conditions for spin-quantitation.

S K-Edge XAS Sample Preparation. For **[1^{Bu,SMe}]⁺** solid samples, CH_2Cl_2 solutions of **1^{Bu,SMe}** oxidized using 1 eq $Ac_2Fc^+SbF_6^-$ at RT under N_2 were evaporated and used without further purification. In an inert atmosphere glove box (less than 0.5 ppm O_2), samples were ground into a fine powder and spread on sulfur-free Kapton tape as thinly as possible to minimize the possibility of self-absorption. The tape was mounted across the window of an aluminum plate, which was affixed inside the sample chamber under a He atmosphere with less than 1.0 ppm O_2 .

XAS data were collected at the Stanford Synchrotron Radiation Lightsource using beamline 4–3 with a fully tuned Si(111) double crystal monochromator and a Rh-coated harmonic rejection mirror under ring conditions of 180–200 mA and 3.0 GeV. All S K-edge measurements were taken at RT and measured in fluorescence mode with a Lytle detector. All data were externally calibrated assigning the first feature in the S K-edge spectrum of $Na_2S_2O_3$ to 2472.02 eV. Calibration scans were collected before and after every sample to ensure beamline calibration accuracy. In all cases the shift in calibration was less than 0.1 eV. Typically three scans were collected of each sample and averaged to provide reproducibility and to decrease the noise level of the data. A smooth linear background was fit to the pre-edge region and removed from the entire spectrum of the averaged data. The data were normalized to an edge jump of 1.0 at 2470 eV. The pre-edge and whiteline features of the data (2469–2477 eV) were fit using Edg_Fit, part of the EXAFSPAK program suite.³² The data were fit using features comprised of a 1:1 mixture of Lorentzian to Gaussian lineshapes. For each feature in each fit, the energy, amplitude and half-width were allowed to vary. In all cases, a minimum number of features were used that successfully fit both the data and the second derivative of the data. Values reported for peak areas are calculated as peak amplitude times full-width at half-max. The %S hole values were evaluated in accordance with previous reported procedures.^{9,33,34}

RESULTS AND ANALYSIS

1. Synthesis. Two equivalents of 3-*tert*-butyl-5-methoxysalicylaldehyde³¹ or 3-*tert*-butyl-5-isopropylsulfanylsalicylaldehyde were condensed with racemic *trans*-1,2-diaminocyclohexane to prepare **3^{OMe2}** or **3^{SPr2}**, respectively (Scheme 3). Reduction of either diimine with sodium cyanoborohydride in acetic acid gave ligands **4^{OMe2}** and **4^{SPr2}** in high yields.³⁵ Metalation of these ligands using anhydrous $CuCl_2$ and NEt_3 proceeded with high yields of the corresponding symmetric copper complexes: **1^{SPr2}**, **1^{OMe2}**, **2^{SPr2}**, and **2^{OMe2}**. For the latter two complexes, there is a concern of possibly auto-oxidizing the $ArCH_2-NHCy$ bonds. In nickel(II) and cobalt(II) complexes of similar ligands, aerobic oxidation of these bonds is facile.³⁶ This was avoided by using a rapid metalation procedure, and no undesirable oxidation was apparent in characterization of the products. **1^{Bu2}** and **2^{Bu}** were synthesized as previously reported.^{9,25}

Construction of nonsymmetric ligands was achieved by condensing the first equivalent of salicylaldehyde with the monohydrochloride salt of racemic *trans*-1,2-diaminocyclohexane.¹³ The second condensation is slowed considerably and the monoimine products (**A** or **B**, Scheme 3) can be isolated in good yield. Addition of triethylamine with the second equivalent of salicylaldehyde deprotonates the hydrochloride salt and allows six nonsymmetric ligands **3^{R1,R2}** ($R_1, R_2 = 'Bu, S'Pr, OMe$) to be formed. Reduction of **3^{R1,R2}** with sodium cyanoborohydride in acetic acid gave **4^{R1,R2}** in high yields. The methods used for introduction of copper into the symmetric ligands were also used for the nonsymmetric ligands. To forestall salicylaldehyde exchange, metalation of **3^{R1,R2}** was

performed under anhydrous conditions (ether/methanol) that rapidly precipitate $1^{R_1,R_2}$.

2. UV-Vis Spectroscopy of Neutral Complexes. The neutral complexes $1^{R_1,R_2}$ have nearly identical absorption spectra containing an envelope of $d-d$ transitions near 17500 cm^{-1} (570 nm), an intense near-UV band near 26000 cm^{-1} arising from a combination of phenolate-copper(II) ligand-to-metal charge transfer (LMCT) and/or Schiff base $\pi-\pi^*$ transitions, and UV absorptions arising from the aromatic moieties (Figure 2). The neutral forms of $2^{R_1,R_2}$ also have similar UV-vis spectra, the main features being the $d-d$ envelope near 16500 cm^{-1} and phenolate-copper(II) LMCT bands near 23000 cm^{-1} ; both absorptions are red-shifted in the bis-methoxy complex, 2^{OMe_2} .

3. EPR Spectroscopy of Neutral Complexes. Frozen solution EPR spectra (Figure S1, Supporting Information) of these complexes (CH_2Cl_2 , 77 K) are very similar among the $1^{R_1,R_2}$ and $2^{R_1,R_2}$ series and can be simulated with the same set of g values and hyperfine coupling constants ($1^{R_1,R_2}$: $g_{\parallel} = 2.19$, $g_{\perp} = 2.04$, $A_{\parallel} = 205\text{ G}$, $A_{\perp} \approx 30\text{ G}$, $A_{\perp}^N \approx 15\text{ G}$; $2^{R_1,R_2}$: $g_{\parallel} = 2.21$, $g_{\perp} = 2.04$, $A_{\parallel} = 190\text{ G}$, $A_{\perp} \approx 40\text{ G}$, $A_{\perp}^N \approx 8\text{ G}$; A_{\perp} is not resolved in all cases due to broadening). These spectroscopic results indicate that all $1^{R_1,R_2}$ and $2^{R_1,R_2}$ exist as monomeric, nearly planar complexes with the intended homology of coordination around the copper center.

4. Electrochemistry. Results from differential pulse voltammetry (DPV, Figure 1) indicate that all of the complexes display two phenolate-based oxidation processes at potentials near or greater than the $\text{Fc}^{0/+}$ redox couple (0 mV) to form copper(II)-phenoxy monocations ($[1^{R_1,R_2}]^+$, $[2^{R_1,R_2}]^+$) and copper(II)-bis(phenoxy) dications ($[1^{R_1,R_2}]^{2+}$, $[2^{R_1,R_2}]^{2+}$).³⁷

In general, the oxidation potentials for complexes $1^{R_1,R_2}$ are higher than those of $2^{R_1,R_2}$ by ca. 350 mV (Table 1). The reduction of the electron-withdrawing imines in $1^{R_1,R_2}$ to amines in $2^{R_1,R_2}$ makes the phenolates easier to oxidize. Among the symmetric complexes ($R_1 = R_2$), those bearing $-\text{OMe}$ groups are oxidized at lower potentials than those bearing $-\text{S}^i\text{Pr}$ groups. This order matches the electron-donating properties expected from Hammett σ^+ constants of these substituents.³⁸

For the nonsymmetric complexes ($R_1 \neq R_2$), the two redox couples observed can be correlated to the sequential oxidation of the two phenolates: the more electron-rich phenolate at the lower potential and the less electron-rich phenolate at the higher potential.

5. UV-Vis-NIR Spectroscopy of Phenoxy Complexes. Spectrophotometric titrations of $1^{R_1,R_2}$ and $2^{R_1,R_2}$ with $\text{Th}^+\text{SbF}_6^-$ ($E^\circ = +890\text{ mV vs Fc}^+/\text{Fc}$) in CH_2Cl_2 result in the formation of one- and two-electron oxidized complexes: $[1^{R_1,R_2}]^{+/2+}$ and $[2^{R_1,R_2}]^{+/2+}$ (Figure 2).³⁹⁻⁴¹ The use of low dielectric solvent (CH_2Cl_2) precludes complex dissociation as evidenced by the reversibility of the oxidations by titrations with ferrocene.

Spectra of $[1^{R_1,R_2}]^{+/2+}$ and $[2^{R_1,R_2}]^{+/2+}$ are particularly useful for identifying UV-vis spectroscopic signatures of $-\text{OMe}$ and $-\text{S}^i\text{Pr}$ substituted phenoxy. The spectrum of $[1^{\text{OMe}_2}]^+$ contains a pair of intense, narrow transitions near 21400 and 22700 cm^{-1} , which resemble those seen previously for *para*-OMe complexes;⁴² upon double oxidation to $[1^{\text{OMe}_2}]^{2+}$, these absorptions roughly double in intensity, corresponding to formation of two coordinated phenoxy.⁴²

A similar pair of absorptions is seen in the spectra of $[2^{\text{OMe}_2}]^+$ and $[2^{\text{OMe}_2}]^{2+}$ near 23400 and 24400 cm^{-1} , respectively. These transitions appear near 16500 and 17500 cm^{-1} in the spectra

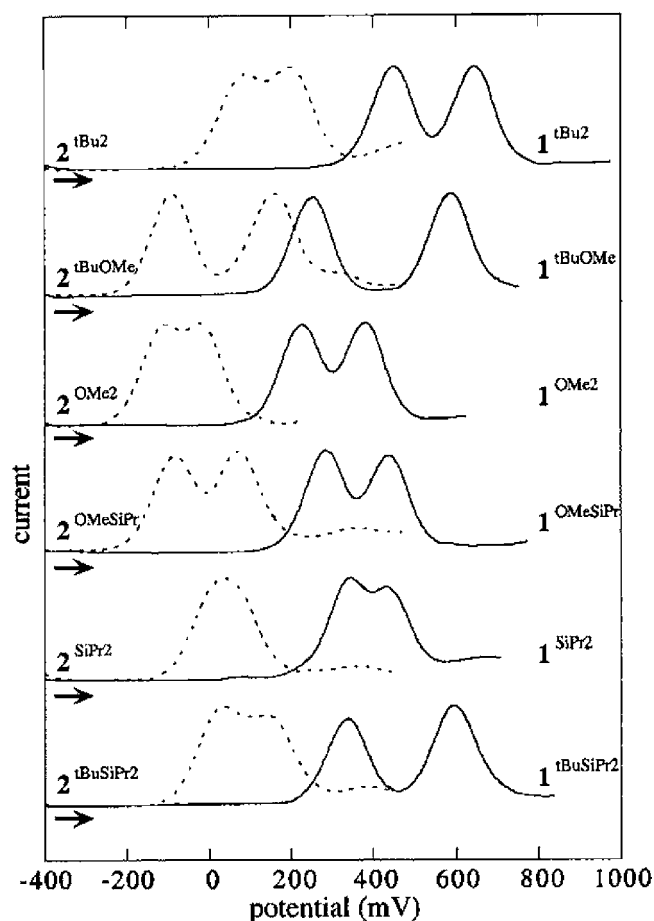


Figure 1. Differential pulse voltammograms of copper complexes $1^{R_1,R_2}$ (solid lines) and $2^{R_1,R_2}$ (dotted lines). Conditions: CH_2Cl_2 with $0.1\text{ M Bu}_4\text{NClO}_4$, 1 mM Cu vs $\text{Fc}^{0/+}$.

Table 1. Electrochemical Data for Copper Complexes $1^{R_1,R_2}$ and $2^{R_1,R_2}$

complex	E_1 (mV)	E_2 (mV)	E_{ave} (mV)	ΔE (mV)	K_c
1^{tBu_2}	450	650	550	200	2500
1^{tBuOMe}	250	590		340	6×10^5
1^{OMe_2}	240	400	320	160	500
1^{OMeSiPr}	280	435		155	400
1^{SiPr_2}	340	440	385	110	70
1^{tBuSiPr}	340	595		255	2×10^4
2^{tBu_2}	80	210	145	130	160
2^{tBuOMe}	-90	160		250	2×10^4
2^{OMe_2}	-120	-10	-65	110	70
2^{OMeSiPr}	-90	70		160	500
2^{SiPr_2}	10	80	45	70	15
2^{tBuSiPr}	25	150		125	130

of $[1^{\text{SiPr}_2}]^{+/2+}$ and $[2^{\text{SiPr}_2}]^{+/2+}$, respectively, leading to deep blue and purple colors in solution. The intensity of these absorptions in the spectra of $[1^{\text{SiPr}_2}]^{2+}$ and $[2^{\text{SiPr}_2}]^{2+}$ is ca. double that observed in the spectra of $[1^{\text{SiPr}_2}]^+$ and $[2^{\text{SiPr}_2}]^+$, supporting their assignment as intraring sulfur-aryl $\pi-\pi^*$ transitions. Complexes with *ortho*-methylsulfanylphenoxy groups give rise to similar transitions, albeit at lower energies and with lesser intensity.^{43,44} Intense absorptions in the UV region (ca. 29000 cm^{-1}) also appear to be characteristic of the $-\text{S}^i\text{Pr}$ substituted phenoxy.

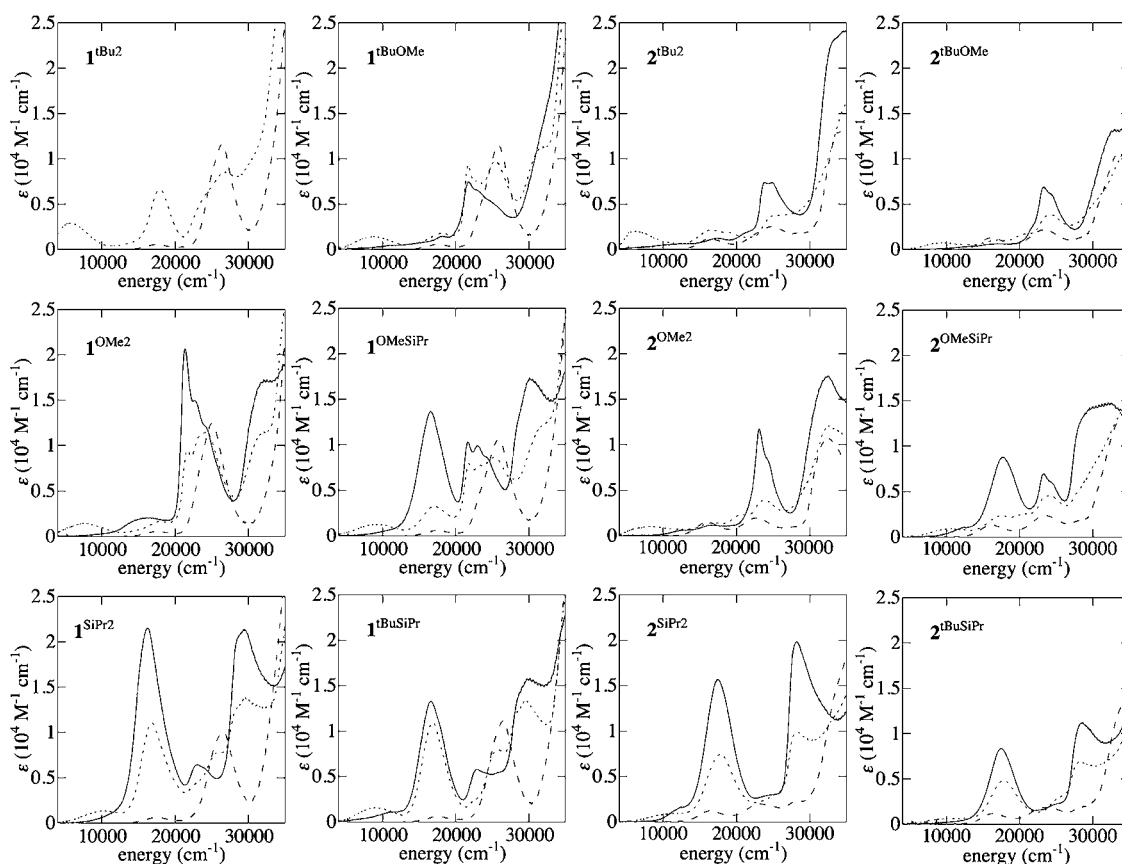


Figure 2. UV-vis-NIR spectra of $1^{R_1,R_2}$ and $2^{R_1,R_2}$ (dashed), $[1^{R_1,R_2}]^+$ and $[2^{R_1,R_2}]^+$ (dotted), and $[1^{R_1,R_2}]^{2+}$ and $[2^{R_1,R_2}]^{2+}$ (solid) in CH_2Cl_2 .

The absorption spectra of the nonsymmetric complexes contain similar aryl $\pi-\pi^*$ transitions as the symmetric complexes, and the energy of these transitions indicate the sequence in which the different phenolates are oxidized. For example, the spectrum of $[1^{\text{OMe},\text{S}^i\text{Pr}}]^+$ shows intense features associated with a -OMe substituted phenoxy near 21800 and 23000 cm^{-1} and little intensity near 16000 cm^{-1} , the region expected for an -SⁱPr substituted phenoxy; the -OMe substituted phenolate is oxidized preferentially (Figure 3a). Upon two-electron oxidation to $[1^{\text{OMe},\text{S}^i\text{Pr}}]^{2+}$, the aryl $\pi-\pi^*$ transitions associated with both -OMe and -SⁱPr substituted phenoxy are observed near 22000 and 16000 cm^{-1} , respectively; the spectrum of $[1^{\text{OMe},\text{S}^i\text{Pr}}]^{2+}$ is intermediate between those of $[1^{\text{S}^i\text{Pr}_2}]^{2+}$ and $[1^{\text{OMe}_2}]^{2+}$ (Figure 3b).

One-electron oxidation of $1^{\text{tBu},\text{S}^i\text{Pr}}$ gives rise to a sulfur-aryl $\pi-\pi^*$ absorption near 16800 cm^{-1} (Figure 2); after a second oxidation to form $[1^{\text{tBu},\text{S}^i\text{Pr}}]^+$, the -tBu substituted phenoxy contributes significant intensity to the UV phenoxy absorption near 22900 cm^{-1} and a lesser amount to the feature near 16800 cm^{-1} .

In complexes $2^{R_1,R_2}$, a lesser distinction exists in the two sequential phenolate oxidations, and the spectra of $[2^{R_1,R_2}]^+$ are generally intermediate between those of $2^{R_1,R_2}$ and $[2^{R_1,R_2}]^{2+}$ in the UV-visible region. The spectra of the $[2^{R_1,R_2}]^{2+}$ dications do contain absorptions from both phenoxy moieties: that of $[2^{\text{OMe},\text{S}^i\text{Pr}}]^{2+}$ has both near-UV $\pi-\pi^*$ absorption of the -OMe substituted phenoxy and the visible sulfur-aryl CT absorption of the -SⁱPr substituted phenoxy (Figure 2).

NIR absorption (5000–11000 cm^{-1}) are observed for the monocations, $[1^{R_1,R_2}]^+$ and $[2^{R_1,R_2}]^+$, but not the neutral or two-

electron oxidized forms. Due to the energy range and intensities of these absorptions ($\epsilon = 700\text{--}2000 \text{ M}^{-1} \text{ cm}^{-1}$) and their association with the mixed-valent monocations $[1^{R_1,R_2}]^+$ and $[2^{R_1,R_2}]^+$, these absorptions are assigned to phenolate-phenoxy IVCT bands. Among the symmetrically substituted complexes, the maximum of the IVCT absorption increases in the order -OMe < -SⁱPr < -tBu, and the energies of the analogous $1^{R_1,R_2}$ and $2^{R_1,R_2}$ complexes are very similar. In contrast to the substituent-characteristic behavior seen for the UV and visible absorptions, the NIR absorptions of the oxidized nonsymmetric complexes show no simple relationship to those of the symmetric precursors.

Most of the NIR absorptions of the $[1^{R_1,R_2}]^+$ and $[2^{R_1,R_2}]^+$ overlap with visible absorptions, so the UV-vis-NIR spectra were fit with multiple Gaussians to obtain the energy (ν_{max}), intensity (ϵ_{max}), and half-width ($\Delta\nu_{1/2}$) of the IVCT transitions (Figure 4, Table 2).⁴⁵ Comparison of $\Delta\nu_{1/2}$ to the bandwidth in the high temperature limit ($\Delta\nu_{\text{HTL}}$) predicted by eq 3 (below) shows that $\Delta\nu_{1/2}$ is greater than $\Delta\nu_{\text{HTL}}$ in all cases, supporting their assignment as IVCT bands.^{28,46}

The electronic coupling coefficients, H_{AB} , were evaluated using the band-shape parameters and eq 4 (below). The oxygen-oxygen distance, r_{OO} , is the approximate electron transfer distance and values from the crystal structures of $[1^{\text{tBu}_2}]^+$ and $[1^{\text{OMe}_2}]^+$ were used for $[1^{R_1,R_2}]^+$ and $[2^{R_1,R_2}]^+$ (ca. 2.7 Å).^{24,47} Comparison of H_{AB} for all $[1^{R_1,R_2}]^+$ shows that the values cluster around $2100 \pm 200 \text{ cm}^{-1}$ despite the wide range of ν_{max} (5700–10200 cm^{-1}). Similarly, all $[2^{R_1,R_2}]^+$ complexes have H_{AB} values centered around $1800 \pm 200 \text{ cm}^{-1}$. Previous work suggests that the actual electron transfer distance

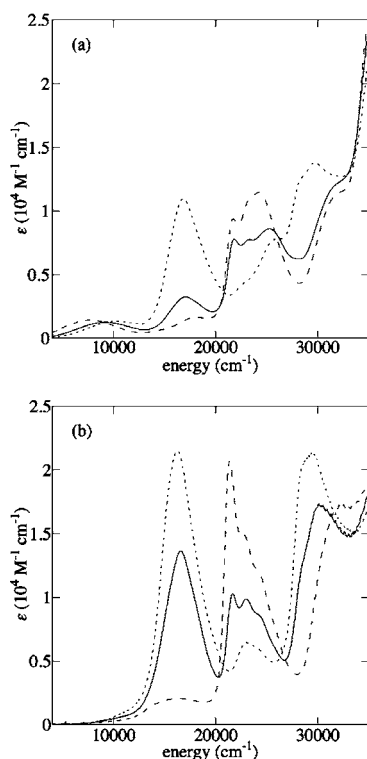


Figure 3. (a) UV-vis-NIR spectra of $[1^{OMe_2}]^+$ (dashed line), $[1^{S^Pr_2}]^+$ (dotted line), and $[1^{OMe,S^Pr}]^+$ (solid line). (b) UV-vis-NIR spectra of $[1^{OMe_2}]^{2+}$ (dashed line), $[1^{S^Pr_2}]^{2+}$ (dotted line), and $[1^{OMe,S^Pr}]^{2+}$ (solid line).

will vary slightly between the different complexes, but this is not expected to influence the H_{AB} to a large extent (ca. $\pm 200 \text{ cm}^{-1}$).⁹ The similarities of H_{AB} for all $[1^{R_1,R_2}]^+$ or $[2^{R_1,R_2}]^+$ imply that the phenolate-phenoxyl coupling is similar for all the peripheral substituents.

6. EPR Spectroscopy of Phenoxyl Complexes. X-band EPR spectra were obtained for 0.1 mM frozen (77 K) CH_2Cl_2 solutions of $[1^{R_1,R_2}]^{0/+2+}$ or $[2^{R_1,R_2}]^{0/+2+}$ (Figure S1, Supporting Information). Despite the similarities of the EPR spectra of $1^{R_1,R_2}$ and $2^{R_1,R_2}$, significant substituent-dependent differences exist between the spectra of their one- and two-electron oxidized derivatives. Among one and two-electron oxidized species, $[1^{OMe_2}]^+$ and $[2^{OMe_2}]^+$ best follow the literature precedent as these copper(II)-phenoxyl complexes are EPR silent relative to the neutral forms. No half-field signals associated with a triplet species were observed for the one-electron oxidized complexes. In the former case, a large zero-field splitting parameter is thought to render the one-electron oxidized species EPR silent at X-band frequencies.²⁴

$[1^{OMe_2}]^{2+}$ uniquely possesses a broad EPR signal that closely resembles an $S = 3/2$ spectrum reported for a tacn-bridged copper(II)-bis(phenoxyl) complex (Figure S2, Supporting Information).⁴² The other two-electron oxidized complexes show low intensity isotropic signals near $g = 2.0$, which could be attributed to $S = 1/2$ species. The spectrum of $[1^{tBu,OMe}]^{2+}$ most likely represents a copper-containing decay product, as this species is unstable at room temperature, at which it was prepared.

The EPR spectra for oxidized complexes bearing at least one $-S^iPr$ substituent have markedly different behavior. One-electron oxidation does not result in a loss of EPR intensity, rather, the

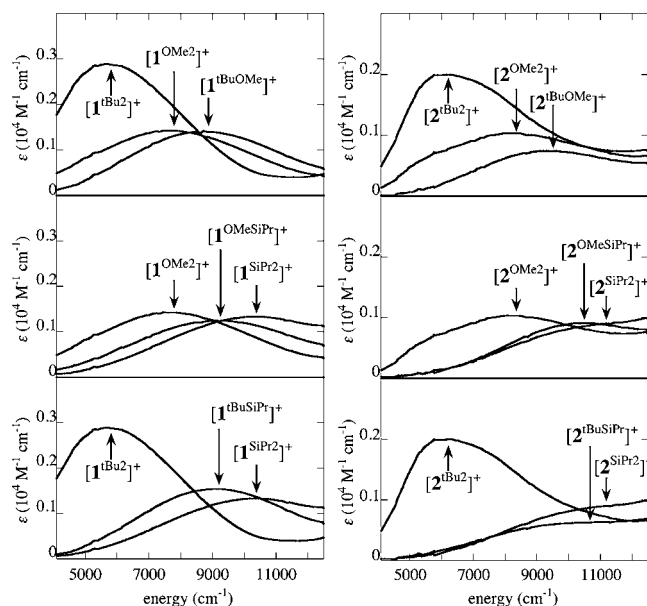


Figure 4. Comparison of NIR absorptions for symmetric and nonsymmetric $[1^{R_1,R_2}]^+$ and $[2^{R_1,R_2}]^+$.

Table 2. IVCT Analysis for $[1^{R_1,R_2}]^+$ and $[2^{R_1,R_2}]^+$

complex	ν_{\max} ^a (cm^{-1})	ϵ ($\text{M}^{-1}\text{cm}^{-1}$) ^a	$\Delta\nu_{1/2}$ ^a (cm^{-1})	$\Delta\nu_{\text{HTT}}$ ^b (cm^{-1})	H_{AB} ^c (cm^{-1})
$[1^{tBu_2}]^+$	5700	2900	5600	3600	2300
$[1^{tBu,OMe}]^+$	8700	1400	5300	4500	1900
$[1^{OMe_2}]^+$	7800	1400	6200	4200	2000
$[1^{OMe,S^Pr}]^+$	9300	1200	6300	4600	2000
$[1^{S^Pr_2}]^+$	10200	1300	6200	4900	2200
$[1^{tBu,S^Pr}]^+$	9300	1600	5800	4600	2200
$[2^{tBu_2}]^+$	6300	2000	6200	3800	2100
$[2^{tBu,OMe}]^+$	9600	700	5400	4700	1500
$[2^{OMe_2}]^+$	8300	1000	6200	4400	1700
$[2^{OMe,S^Pr}]^+$	10500	900	5600	4900	1800
$[2^{S^Pr_2}]^+$	11200	900	6400	5100	2000
$[2^{tBu,S^Pr}]^+$	10600	600	6900	4900	1600

^aDetermined by multiple Gaussian fitting of the UV-vis-NIR spectra.

^bFrom eq 3. ^cFrom eq 4.

signals broaden considerably and the spin integration remains relatively constant to that of their parent neutral forms. $1^{OMe,S^Pr}$ does show a reduction in intensity when oxidized, but oxidation is centered preferentially on the $-OMe$ substituted phenolate in this case. Double oxidation of the $-S^iPr$ containing complexes reduces the intensity of their EPR signals, but spectra are still dominated in most cases by low intensity broad isotropic signals near $g = 2.0$.

7. Sulfur K-Edge XAS. Sulfur K-edge XAS spectra of neutral and one-electron oxidized $1^{tBu,SMe}$ display intense edge features near 2472 eV (Figure 5). The edge feature of $[1^{tBu,SMe}]^+$ occurs at higher energy in comparison to $1^{tBu,SMe}$, consistent with an increase in sulfur effective nuclear charge (Z_{eff}) upon oxidation.⁴⁸ In addition, a new pre-edge feature is apparent in the spectra of $[1^{tBu,SMe}]^+$ at ca. 2471 eV. Analysis of the pre-edge feature using methods published previously yields a sulfur contribution to the phenoxyl hole of 7% for $[1^{tBu,SMe}]^+$, consistent with preferential oxidation of the $-SMe$ substituted phenolate, and an orientation of the $-SMe$ group in-plane with the phenolate ring.⁹

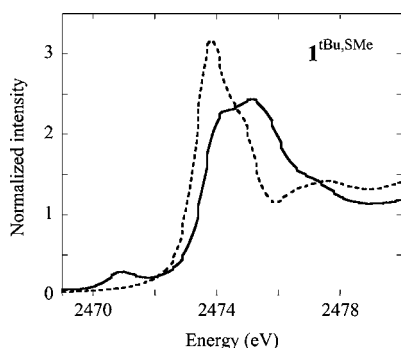


Figure 5. Normalized sulfur K-edge XAS spectra of (dotted) $1^{\text{Bu,SMe}}$ and (solid) $[1^{\text{Bu,SMe}}]^+$.

DISCUSSION

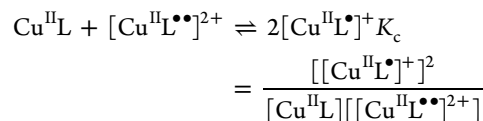
In this study of complexes 1^{R_1R_2} and 2^{R_1R_2} bearing dissimilar substituents on their periphery, the expected differentiation of the phenolate moieties is observed in both electrochemical and spectrophotometric experiments. Reversible oxidations of the phenolates are well-distinguished when an inherent thermodynamic difference exists between their redox potentials, and the sequential oxidations of the two phenolates induce characteristic absorptions associated with the methoxy substituent in the near-UV and with the sulfanyl substituent in the visible region. The *para*-substituents were not expected to disturb the spin distribution of the radical species generated by one- and two-electron oxidation, yet the EPR experiments suggest that a connection does exist that is particularly strong for the sulfanyl substituent, presumably due to the larger interspin distance afforded by significant delocalization of the hole onto the *para*-sulfur atoms, leading to weaker electron–electron coupling and more diradical EPR character.^{9,49}

S K-edge XAS is a complementary technique to probe the sulfur contribution to the phenoxyl hole in $[1^{\text{Bu,SMe}}]^+$, the complex most structurally relevant to GO_{ox} . The edge feature at ca. 2474 eV observed for the neutral complex is consistent with other thioether compounds and a shift to higher energy for the one-electron oxidized species is consistent with an increase in sulfur Z_{eff} . The presence of an additional pre-edge feature in the spectra of $[1^{\text{Bu,SMe}}]^+$ is attributed to a S_{1s} to phenoxyl SUMO transition, the intensity of which reflects the degree of S *p*-orbital mixing into the SUMO.^{9,48} The degree of delocalization observed for $[1^{\text{Bu,SMe}}]^+$ (7%) is consistent with other spectroscopic and electrochemical results that indicate preferential oxidation of the -SMe bearing phenolate. This result is similar to that reported for the symmetric $[1^{\text{SMe}_2}]^+$ (13%).⁹ It is curious that a halving of the number of sulfur atoms corresponds to an approximate halving of the S radical character as determined by XAS. Whether this corresponds to a true electronic effect or possible decay of $[1^{\text{Bu,SMe}}]^+$ has yet to be determined.

Comparison of the electrochemical potentials of the nonsymmetric complexes to those of the symmetric congeners shows that sequential oxidation of the thermodynamically differentiated phenolates can be observed. For 1^{OMe_2} , $1^{\text{Bu,OMe}}$, and $1^{\text{OMe,S}^i\text{Pr}}$, the first oxidation potential corresponds to the oxidation of the -OMe substituted phenolate, as indicated by the growth of the 22000 cm^{-1} feature in the UV–vis spectrum of the one-electron oxidized forms (Figure 2). The redox

potential for the first oxidation of these complexes increases in the order $1^{\text{OMe}_2} < 1^{\text{Bu,OMe}} < 1^{\text{OMe,S}^i\text{Pr}}$, a trend that does not correspond directly to the electron-donating ability of the substituent on the unoxidized phenolate (i.e., $\text{OMe} > \text{S}^i\text{Pr} > \text{Bu}$).

The mixed-valence, monocations $[1^{\text{R}_1\text{R}_2}]^+$ and $[2^{\text{R}_1\text{R}_2}]^+$ exist in equilibrium with a mixture of their respective neutral and dicationic forms:



The comproportionation constant K_c is determined at 298 K by $\log K_c = (\Delta E/59 \text{ mV})$ (Table 1). ΔE values larger than a statistical value of 36 mV ($K_c = 4$)^{50,51} imply that a thermodynamic stabilization of the monocationic species exists. Based predominantly on results from bimetallic mixed-valence systems, the free energy of comproportionation ($\Delta G_c = -nF\Delta E$) can be separated into a statistical component ($\Delta G_s = 36 \text{ mV} = 290 \text{ cm}^{-1}$), electrostatic repulsions (ΔG_e), inductive effects (ΔG_i), mixed-valence resonance stabilization (ΔG_r), antiferromagnetic exchange (ΔG_{ex}) and ion pairing (ΔG_{ip}):^{51,52} ΔG_r , the resonance stabilization, is generally thought to dominate ΔG_c .

$$\Delta G_c = \Delta G_s + \Delta G_e + \Delta G_i + \Delta G_r + \Delta G_{\text{ex}} + \Delta G_{\text{ip}} \quad (1)$$

In a symmetric Marcus–Hush model, if the two uncoupled states have minima at $E = 0$, the coupled ground state energy surface has a minimum at $E_{\text{min}} = -H_{\text{AB}}^2/\lambda$. This value corresponds to a per-molecule stabilization rendered by delocalization ($\Delta G_r' = E_{\text{min}}$) and is therefore counted twice for the comproportionation since two mixed-valent molecules are formed per reaction ($\Delta G_r = 2\Delta G_r' = -2H_{\text{AB}}^2/\lambda$).

When ΔG_c is plotted versus $1/\lambda$ (λ derived from NIR absorption bands) for symmetric 1^{R_1R_2} and 2^{R_1R_2} complexes (Figure 6), a linear correlation is indeed found. The slopes

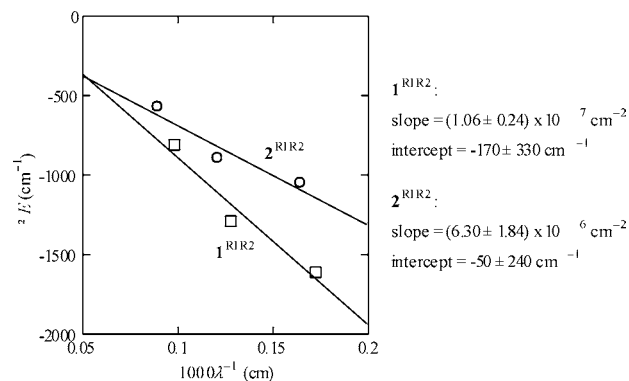


Figure 6. Plots of the electrochemical splitting (ΔE) versus $1/\lambda$ for 1^{R_1R_2} (squares) and 2^{R_1R_2} (circles), shown with linear fits.

of linear fits of the data can be evaluated to give $H_{\text{AB}} = 2300 \pm 300 \text{ cm}^{-1}$ and $1800 \pm 300 \text{ cm}^{-1}$ for 1^{R_1R_2} and 2^{R_1R_2} , respectively. Small values of the intercepts and small residuals support the assumptions that other ΔG factors are small and that ΔG_c is dominated by ΔG_r . Furthermore, the good correlation indicates that H_{AB} is unchanged by peripheral substitution and independently confirms the magnitude of the coupling terms as determined by Hush analysis of the NIR transitions (Table 2).

For a symmetric two-redox center system, the two states that correspond to localization of the unpaired electron completely on one redox moiety or the other are modeled by harmonic functions representing molecular vibrations that map onto the electron transfer coordinate. These two diabatic states couple to form two adiabatic energy surfaces (Figure 7a): a ground state surface whose two minima represent a partial localization of charge on each redox center, and an excited state surface with a single minimum. The IVCT band corresponds to transition between the two adiabatic states, and ν_{\max} , ϵ_{\max} and $\Delta\nu_{1/2}$ of this transition are related to the reorganizational energy of the system (λ) subsequent to electron transfer and H_{AB} . For IVCT transitions, the absorption bandwidth is expected to increase with ν_{\max} and $\Delta\nu_{HTL}$ given by eq 3. Importantly H_{AB} can be determined experimentally from the ν_{\max} , ϵ_{\max} and $\Delta\nu_{1/2}$ of the IVCT band and an estimate of the electron transfer distance r_{CT} using the Hush equation (eq 4, Table 2).

$$\begin{vmatrix} \lambda x^2 - E & H_{AB} \\ H_{AB} & \lambda(1-x^2) + \Delta G^\circ - E \end{vmatrix} = 0 \quad (2)$$

$$\Delta\nu_{HTL} = \sqrt{16\ln 2RT\nu_{\max}} = \sqrt{2310\nu_{\max}} \quad (3)$$

$$H_{AB} = 2.06 \times 10^{-2} \frac{\sqrt{\epsilon_{\max}\Delta\nu_{1/2}\nu_{\max}}}{r_{CT}} \quad (4)$$

To extend the Marcus–Hush model for complexes with nonsymmetric phenolate moieties (i.e., $1^{R_1,R_2}$ and $2^{R_1,R_2}$), the secular equation that defines the ground and excited state surfaces is perturbed by the addition of ΔG° , a term that represents the thermodynamic free energy difference between the two localized states (eq 2). For the nonsymmetric model, the two minima of the ground state surface now lie at different energies (Figure 7b), with the unpaired electron preferentially localized on the ring with the lower binding energy. The energy of the IVCT absorption becomes the sum of the reorganizational energy λ and ΔG° . Equations 3 and 4 for determining $\Delta\nu_{HTL}$ and H_{AB} are applicable for both the nonsymmetric and symmetric models.

In nonsymmetric, mixed-valence Ru dimers and bis-(triarylamine) compounds, the approximation $\Delta E = \Delta G^\circ$ works reasonably well when applied to correlating the energies of their IVCT absorptions.^{53,54} However ΔE for the nonsymmetric complexes $[1^{R_1,R_2}]^+$ and $[2^{R_1,R_2}]^+$ depends not only on the difference in potentials between the two phenolates (ΔG° , estimable at 100–200 mV) but also on the splitting engendered by resonance stabilization (ΔG_r , 70–200 mV). In the nonsymmetric case, an expression for ΔG_r will be dependent on ΔG° . Rather than attempt a self-consistent solution for these two values, the redox potentials of the symmetric complexes should serve as references. The average of E_1^R and E_2^R ($= E_{ave}^R$) for symmetric $1^{R_1,R_2}$ and $2^{R_1,R_2}$ complexes ($R_1 = R_2 = R$) can be taken as an estimate of E^R , the inherent redox potential of an R-substituted phenolate. The thermodynamic difference in a nonsymmetric complex ($R_1 \neq R_2$) is then $\Delta G^\circ = E_{ave}^{R_1} - E_{ave}^{R_2}$.

The energy of an IVCT absorption of a nonsymmetric compound “ R_1R_2 ” is expected to be the sum of its reorganizational energy ($\lambda_{R_1R_2}$) and the separation of the ground state energies of the two charge-localized states ($\Delta G^\circ_{R_1R_2}$). If the reorganizational energies for self-exchange of complexes R_1R_1 and R_2R_2 are known, $\lambda_{R_1R_2}$ is estimated by the average of those energies

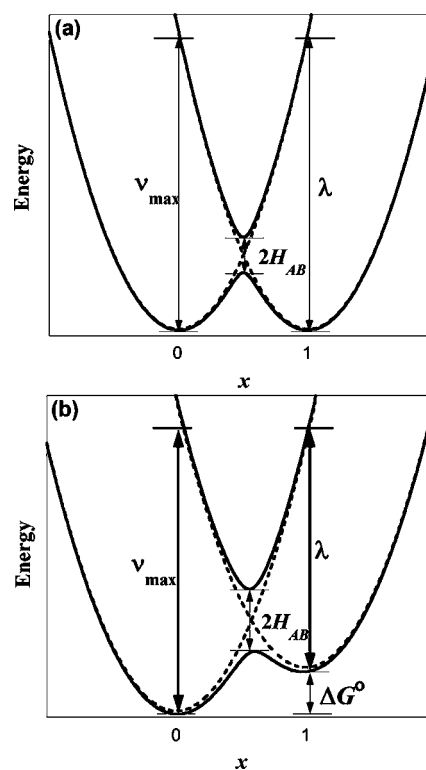


Figure 7. (a) Scheme of Marcus–Hush coupling in symmetric mixed-valence complexes. (b) Scheme of Marcus–Hush coupling in nonsymmetric mixed-valence complexes. The energy of the IVCT absorption corresponds to $\lambda + \Delta G^\circ$.

$(\lambda_{R_1R_1} + \lambda_{R_2R_2})/2$ in the classic Marcus cross-relation.⁵⁵ Using the ΔG° expression derived above, the ultimate expression used to correlate the NIR transition energy of the nonsymmetric (R_1R_2) mixed-valence complex to the properties of the corresponding symmetric (R_1R_1 , R_2R_2) complexes is then:

$$\nu_{R_1R_2} = \lambda_{R_1R_2} + \Delta G^\circ_{R_1R_2} = \left(\frac{\lambda_{R_1R_1} + \lambda_{R_2R_2}}{2} \right) + |E_{ave}^{R_1} - E_{ave}^{R_2}| \quad (5)$$

As expected for a symmetric complex ($R_1 = R_2 = R$), this expression simplifies to $\nu_{RR} = \lambda_{RR}$. The reorganizational energies (5000–10000 cm^{-1}) are significantly larger than the differences in redox potentials (100 mV = 800 cm^{-1}), so the $\lambda_{R_1R_2}$ term will tend to dominate overall. The necessary variables and results for the application of eq 5 to the six mixed-substituent complexes in this study are listed in Table 3.

Table 3. Correlation of NIR Transition Energies of Nonsymmetric ($R_1 \neq R_2$) to Symmetric ($R_1 = R_2$) Substituted Mixed-Valence Complexes

complex	λ_{R_1} (cm^{-1})	λ_{R_2} (cm^{-1})	$ E_{R_1} - E_{R_2} $ (mV)	$ E_{R_1} - E_{R_2} $ (cm^{-1})	$\nu_{R_1R_2}$ (cm^{-1})	ν_{\max} (cm^{-1})
$[1^{Bu,OMe}]^+$	5700	7800	230	1850	8600	8700
$[1^{Bu,S^iPr}]^+$	5700	10200	165	1330	9280	9300
$[1^{OMe,S^iPr}]^+$	7800	10200	65	520	9520	9300
$[2^{Bu,OMe}]^+$	6300	8300	210	1690	8990	9600
$[2^{Bu,S^iPr}]^+$	6300	11200	100	810	9560	10600
$[2^{OMe,S^iPr}]^+$	8300	11200	110	890	10640	10500

For $[1^{R_1,R_2}]^+$ ($R_1 \neq R_2$), the agreement between $\nu_{R_1R_2}$ and the experimental value of ν_{\max} is remarkably good, with an average

difference of only 100 cm^{-1} for the three complexes. For $[2^{\text{OMe,S}^{\text{Pr}}}]^+$, the difference between ν_{AB} and ν_{max} is only 140 cm^{-1} , but there are significantly larger discrepancies for $[2^{\text{Bu,OMe}}]^+$ and $[2^{\text{Bu,S}^{\text{Pr}}}]^+$ of 600 cm^{-1} and 1000 cm^{-1} , respectively. These discrepancies are comparable to the size of the $|E^{\text{R}_1} - E^{\text{R}_2}|$ term (Table 3), but would only be corrections to the much larger $\lambda_{\text{R}_1\text{R}_2}$ term; therefore, it seems more likely that there are effects on the reorganizational energy that are more subtle than anticipated.

Given that eq 5 seems to deal with mixed-substituent complexes reasonably well, it is possible to apply it toward analysis of the IVCT band of GO_{ox} itself. The -S^{Pr} substituted phenolates were originally intended to model the Tyr272-Cys228 conjugate and the $\text{-}^{\text{t}}\text{Bu}$ substituted phenolates serve as models of unmodified axial Tyr495, therefore providing estimates of the reorganizational energies of the two tyrosines. The redox potential of tyrosine (i.e., Tyr495) is estimated at 1.0 V vs NHE while the redox potential of modified Tyr272- is reported as 400 mV vs NHE.⁵⁶ The ~ 600 mV difference has been separated into contributions from the cysteine cross-link (ca. -230 mV), a π -stacking interaction with neighboring Trp290 (ca. -330 mV), and the presence of the axial tyrosine, Tyr495 (ca. -50 mV).⁵⁷ Assuming a $\Delta G^{\circ}_{\text{R}_1\text{R}_2}$ term of ca. 600 mV ≈ 4800 cm^{-1} , together with a $\lambda_{\text{R}_1\text{R}_2}$ term derived from λ for $[2^{\text{Bu}_2}]^+$ and $[2^{\text{S}^{\text{Pr}_2}}]^+$ (8800 cm^{-1}), predicts a $\nu_{\text{R}_1\text{R}_2}$ of ca. 13600 cm^{-1} for GO_{ox} , well within the envelope of the broad vis-NIR band of the enzyme. While this analysis is admittedly very approximate, it provides a first estimate from experimental data of the IVCT energy of GO_{ox} .

CONCLUSION

Nonsymmetric substitution of a series of Cu^{II} -phenoxyl complexes results in striking differences in their redox and spectroscopic properties, providing insight into the influence of the cysteine-modified tyrosine cofactor in GO. A Marcus-Hush analysis of the oxidized copper complexes suggests they are best described as Class II mixed-valent. Sulfur K-edge XAS assesses the degree of radical delocalization onto the single sulfur atom of nonsymmetric $[1^{\text{Bu,SMe}}]^+$, complementing other spectroscopic and electrochemical results that suggest preferential oxidation of the -SMe bearing phenolate. Estimates of the thermodynamic free-energy difference between the two localized states (ΔG°) and reorganizational energies ($\lambda_{\text{R}_1\text{R}_2}$) of $[1^{\text{R}_1\text{R}_2}]^+$ and $[2^{\text{R}_1\text{R}_2}]^+$ leads to accurate predictions of the spectroscopically observed IVCT transition energies, and a predicted ν_{max} of ~ 13600 cm^{-1} for GO_{ox} .

ASSOCIATED CONTENT

Supporting Information

EPR data. This material is available free of charge via the Internet at <http://pubs.acs.org>.

AUTHOR INFORMATION

Corresponding Author

*stack@stanford.edu

Notes

The authors declare no competing financial interest.

ACKNOWLEDGMENTS

This work was supported by funding from the NIH (GMS0730 to T.D.P.S.) and from CSU Chico (E.C.W.). We thank Prof. E.I. Solomon for instrument use. We thank Dr. Pratik Verma for helpful discussions. Portions of this research were carried out at SSRL, a national user facility operated by Stanford University on behalf of the U.S. Department of Energy, Office of Basic Energy Sciences.

REFERENCES

- (1) Whittaker, J. W. *Chem. Rev.* **2003**, *103*, 2347.
- (2) Rogers, M. S.; Dooley, D. M. *Curr. Opin. Chem. Biol.* **2003**, *7*, 189.
- (3) Firbank, S. J.; Rogers, M. S.; Wilmot, C. M.; Dooley, D. M.; Halcrow, M. A.; Knowles, P. F.; McPherson, M. J.; Phillips, S. E. V. *Proc. Natl. Acad. Sci. U.S.A.* **2001**, *98*, 12932.
- (4) Ito, N.; Phillips, S. E. V.; Yadav, K. D. S.; Knowles, P. F. *J. Mol. Biol.* **1994**, *238*, 794.
- (5) Rogers, M. S.; Tyler, E. M.; Akyumani, N.; Kurtis, C. R.; Spooner, R. K.; Deacon, S. E.; Tamber, S.; Firbank, S. J.; Mahmoud, K.; Knowles, P. F.; Phillips, S. E. V.; McPherson, M. J.; Dooley, D. M. *Biochemistry* **2007**, *46*, 4606.
- (6) Rokhsana, D.; Dooley, D. M.; Szilagy, R. K. *J. Am. Chem. Soc.* **2006**, *128*, 15550.
- (7) Rokhsana, D.; Dooley, D. M.; Szilagy, R. K. *J. Biol. Inorg. Chem.* **2008**, *13*, 371.
- (8) Lee, Y. K.; Whittaker, M. M.; Whittaker, J. W. *Biochemistry* **2008**, *47*, 6637.
- (9) Verma, P.; Pratt, R.; Storr, T.; Wasinger, E. C.; Stack, T. D. P. *Proc. Natl. Acad. Sci.* **2011**, *108*, 18600.
- (10) Whittaker, M. M.; Duncan, W. R.; Whittaker, J. W. *Inorg. Chem.* **1996**, *35*, 382.
- (11) Taki, M.; Kumei, H.; Nagatomo, S.; Kitagawa, T.; Itoh, S.; Fukuzumi, S. *Inorg. Chim. Acta* **2000**, *300*, 622.
- (12) Thomas, F.; Gellon, G.; Gautier-Luneau, I.; Saint-Aman, E.; Pierre, J. L. *Angew. Chem., Int. Ed.* **2002**, *41*, 3047.
- (13) Campbell, E. J.; Nguyen, S. T. *Tetrahedron Lett.* **2001**, *42*, 1221.
- (14) Sawada, Y.; Matsumoto, K.; Katsuki, T. *Angew. Chem., Int. Ed.* **2007**, *46*, 4559.
- (15) Berkessel, A.; Brandenburg, M.; Leitterstorf, E.; Frey, J.; Lex, J.; Schafer, M. *Adv. Synth. Catal.* **2007**, *349*, 2385.
- (16) Matsumoto, K.; Sawada, Y.; Katsuki, T. *Pure Appl. Chem.* **2008**, *80*, 1071.
- (17) Kleij, A. W. *Eur. J. Inorg. Chem.* **2009**, 193.
- (18) Wen, Y. Q.; Ren, W. M.; Lu, X. B. *Org. Biomol. Chem.* **2011**, *9*, 6323.
- (19) Herrero, C.; Hughes, J. L.; Quaranta, A.; Cox, N.; Rutherford, A. W.; Leibl, W.; Aukauloo, A. *Chem. Commun.* **2010**, *46*, 7605.
- (20) Nakano, K.; Nakamura, M.; Nozaki, K. *Macromolecules* **2009**, *42*, 6972.
- (21) Kochem, A.; Orio, M.; Jarjayes, O.; Neese, F.; Thomas, F. *Chem. Commun.* **2010**, *46*, 6765.
- (22) Kurahashi, T.; Fujii, H. *J. Am. Chem. Soc.* **2011**, *133*, 8307.
- (23) Pratt, R. Ph.D. Thesis, Stanford University, 2004.
- (24) Orio, M.; Jarjayes, O.; Kano, H.; Philouze, C.; Neese, F.; Thomas, F. *Angew. Chem., Int. Ed.* **2010**, *49*, 4989.
- (25) Pratt, R. C.; Stack, T. D. P. *J. Am. Chem. Soc.* **2003**, *125*, 8716.
- (26) Crutchley, R. J. *Adv. Inorg. Chem.* **1994**, *41*, 273.
- (27) D'Alessandro, D. M.; Keene, F. R. *Chem. Soc. Rev.* **2006**, *35*, 424.
- (28) Brunshwig, B. S.; Creutz, C.; Sutin, N. *Chem. Soc. Rev.* **2002**, *31*, 168.
- (29) Storr, T.; Verma, P.; Shimazaki, Y.; Wasinger, E. C.; Stack, T. D. *Chem.—Eur. J.* **2010**, *16*, 8980.
- (30) McGlashen, M. L.; Eads, D. D.; Spiro, T. G.; Whittaker, J. W. *J. Phys. Chem.* **1995**, *99*, 4918.
- (31) Larrow, J. F.; Jacobsen, E. N.; Gao, Y.; Hong, Y. P.; Nie, X. Y.; Zepp, C. M. *J. Org. Chem.* **1994**, *59*, 1939.

(32) George, G. N. EXAFSPAK & EDG_FIT; Stanford Synchrotron Radiation Laboratory, Stanford Linear Accelerator Center; Stanford University, 2000.

(33) DeBeer, S.; Randall, D. W.; Nersissian, A. M.; Valentine, J. S.; Hedman, B.; Hodgson, K. O.; Solomon, E. I. *J. Phys. Chem. B* **2000**, *104*, 10814.

(34) Sarangi, R.; George, S. D.; Rudd, D. J.; Szilagyi, R. K.; Ribas, X.; Rovira, C.; Almeida, M.; Hodgson, K. O.; Hedman, B.; Solomon, E. I. *J. Am. Chem. Soc.* **2007**, *129*, 2316.

(35) Böttcher, A.; Elias, H.; Jäger, E. G.; Langfelderova, H.; Mazur, M.; Müller, L.; Paulus, H.; Pelikan, P.; Rudolph, M.; Valko, M. *Inorg. Chem.* **1993**, *32*, 4131.

(36) Böttcher, A.; Elias, H.; Eisenmann, B.; Hilms, E.; Huber, A.; Kniep, R.; Rohr, C.; Zehnder, M.; Neuberger, M.; Springbord, J. *Z. Naturforsch. B* **1994**, *49*, 1089.

(37) $[1^{tBu2}]^+$ exists in an equilibrium between a Cu^{III} -phenolate and a ferromagnetic Cu^{II} -phenoxyl radical species at room temperature (RT) in solution, displaying the nearly iso-energetic nature of the two species.⁴⁷

(38) Hansch, C.; Leo, A.; Taft, R. W. *Chem. Rev.* **1991**, *91*, 165.

(39) Connelly, N. G.; Geiger, W. E. *Chem. Rev.* **1996**, *96*, 877.

(40) Lee, W. K.; Liu, B.; Park, C. W.; Shine, H. J.; Guzman-Jimenez, I. Y.; Whitmire, K. H. *J. Org. Chem.* **1999**, *64*, 9206.

(41) Halfen, J. A.; Jazdzewski, B. A.; Mahapatra, S.; Berreau, L. M.; Wilkinson, E. C.; Que, L., Jr.; Tolman, W. B. *J. Am. Chem. Soc.* **1997**, *119*, 8217.

(42) Bill, E.; Müller, J.; Weyhermüller, T.; Wieghardt, K. *Inorg. Chem.* **1999**, *38*, 5795.

(43) Itoh, S.; Takayama, S.; Arakawa, R.; Furuta, A.; Komatsu, M.; Ishida, A.; Takamuku, S.; Fukuzumi, S. *Inorg. Chem.* **1997**, *36*, 1407.

(44) Itoh, S.; Taki, M.; Kumei, H.; Takayama, S.; Nagatomo, S.; Kitagawa, T.; Sakurada, N.; Arakawa, R.; Fukuzumi, S. *Inorg. Chem.* **2000**, *39*, 3708.

(45) The NIR transition for $[1^{tBu2}]^+$ could be assigned as a low energy LMCT transition by TD-DFT.⁴⁶

(46) Hush, N. S. *Prog. Inorg. Chem.* **1967**, *8*, 391.

(47) Storr, T.; Verma, P.; Pratt, R. C.; Wasinger, E. C.; Shimazaki, Y.; Stack, T. D. P. *J. Am. Chem. Soc.* **2008**, *130*, 15448.

(48) Martin-Diaconescu, V.; Kennepohl, P. *J. Am. Chem. Soc.* **2007**, *129*, 3034.

(49) Rajca, A. *Chem. Rev.* **1994**, *94*, 871.

(50) Flanagan, J. B.; Margel, S.; Bard, A. J.; Anson, F. C. *J. Am. Chem. Soc.* **1978**, *100*, 4248.

(51) Richardson, D. E.; Taube, H. *Coord. Chem. Rev.* **1984**, *60*, 107.

(52) Al-Noaimi, M.; Yap, G. P. A.; Crutchley, R. J. *Inorg. Chem.* **2004**, *43*, 1770.

(53) Chang, J. P.; Fung, E. Y.; Curtis, J. C. *Inorg. Chem.* **1986**, *25*, 4233.

(54) Lambert, C.; Nöll, G. *J. Chem. Soc., Perkin Trans. 2* **2002**, 2039.

(55) Marcus, R. A.; Sutin, N. *Biochim. Biophys. Acta* **1985**, *811*, 265.

(56) Stubbe, J.; van der Donk, W. A. *Chem. Rev.* **1998**, *98*, 705.

(57) Wright, C.; Sykes, A. G. *J. Inorg. Biochem.* **2001**, *85*, 237.